Charge-density-wave phase transition in $1T$-$TiSe_2$: Excitonic insulator versus band-type Jahn-Teller mechanism

K. Rossnagel, L. Kipp, and M. Skibowski
Institut für Experimentelle und Angewandte Physik, Universität Kiel, D–24098 Kiel, Germany
(Received 13 July 2001; revised manuscript received 27 September 2001; published 21 May 2002)

The influence of the charge-density-wave phase transition on the electronic structure of $1T$-$TiSe_2$ is studied by means of high-resolution angle-resolved photoemission spectroscopy with synchrotron radiation. We find that both the Se $4p$-type valence band maximum at Γ and the Ti $3d$-type conduction band minimum at L are lowered upon cooling. Our photoemission results explain the observed anomalies in the transport data and appear to be consistent with the band-type Jahn-Teller mechanism rather than with excitonic electron-hole interaction.

DOI: 10.1103/PhysRevB.65.235101 PACS number(s): 71.45.Lr, 79.60.−i, 71.18.+y

I. INTRODUCTION

Among the many transition-metal dichalcogenides with charge-density-wave (CDW) instabilities, $1T$-$TiSe_2$ is particularly interesting because it is the only group IVB transition-metal compound showing a structural transformation. Upon cooling down from room temperature, $1T$-$TiSe_2$ undergoes a second-order phase transition at $T_C \approx 200$ K into a commensurate CDW phase associated with a $(2\times2\times2)$ superlattice that forms without the precursor of an incommensurate phase.[1,2] The three CDW vectors are zone boundary wave vectors connecting the Γ point with the L points of the hexagonal Brillouin zone (BZ).

At these high-symmetry points of the BZ the electronic structure, which has extensively been studied both experimentally[3–7] and theoretically,[8–10] exhibits a Se $4p$-type valence-band maximum and a Ti $3d$-type conduction-band minimum, respectively. The overlap between the uppermost p band at Γ and the lowest d band at L was carefully estimated to be smaller than 120 meV,[6] resulting in a relatively small Fermi surface (FS) that consists of a Se $4p$ hole pocket in the center of the BZ and Ti $3d$ electron pockets centered at the L points.

In the lively discussion on the driving force of CDW formation in $1T$-$TiSe_2$ several mechanisms have been proposed. Di Salvo *et al.*[1] were the first to suggest that the simple nesting model, which was shown to account for the CDW's in other low-dimensional materials, also explains the CDW phase transition in $1T$-$TiSe_2$. Dimensionality and the topology of the FS are then particularly important in that the FS must exhibit large parallel portions that can be nested by the spanning wave vector of the CDW. According to this model, electron-lattice interaction will produce the distortion in $1T$-$TiSe_2$, if the Γ-point hole FS and the L-point electron FS are near nesting.[8] In contrast to the nesting model, White and Lucovsky[11] proposed an antiferroelectric transition mechanism in which the CDW formation is the result of a soft phonon inherent to the lattice system itself. Their model was motivated by the observation that the lattice and electronic polarizabilities, as determined from optical reflectivity spectra, are unusually large for $1T$-$TiSe_2$.

A third explanation—the excitonic insulator mechanism—was put forward by Wilson[12,13] and has attracted much more attention than the previous two. Within this model the CDW instability arises from direct Coulomb interaction between the Γ holes and the L electrons: In a semimetal with a very small number of electrons and holes the Coulomb interaction between different carriers is only weakly screened leading to bound states between electrons and holes, i.e., excitons. As a consequence, free carriers are removed from the FS and the semimetal eventually becomes a semiconductor. This semimetal-semiconductor transition, which is necessarily accompanied by a structural distortion that doubles the periodicity of the lattice, of course requires that the band overlap or gap is smaller than the exciton binding energy.[14,15]

Finally, Hughes[16] proposed a band-type Jahn-Teller mechanism based on possible effects of the structural transformation on the d-band electronic energy. Band calculations showed that the lowest lying d-band is slightly lower for transition-metal dichalcogenides of the $2H$-type than for $1T$ materials. Thus, from the observed atomic displacements in the structural phase transition of $1T$-$TiSe_2$, indicating a change in the local coordination from octahedral $(1T)$ towards trigonal prismatic $(2H)$, Hughes expected the Ti $3d$ band to shift downwards reducing the total energy. In contrast to Hughes' suggestion, Whangbo and Canadell[17] later pointed out that within the framework of the Jahn-Teller mechanism the energy lowering giving rise to the structural modulation of $1T$-$TiSe_2$ should not occur in the Ti $3d$ bands but in the Se $4p$ bands and that this p-band energy lowering should be associated with the Ti-Se bond shortening in the observed displacement pattern. On the basis of the band-type Jahn-Teller mechanism Motizuki and co-workers[18–21] developed a microscopic theory that has revealed that strong electron-phonon interaction lies at the heart of the CDW phase transition in $1T$-$TiSe_2$ leading to renormalized electron as well as phonon energies.[22]

Although high-resolution angle-resolved photoelectron spectroscopy (ARPES) data[4,6] agreed with band-structure calculations[21] based on the band-type Jahn-Teller effect, this picture has very recently been questioned by Pillo *et al.*[7] who strongly favored the excitonic insulator mechanism. In their ARPES study, which focused on the temperature dependence of the Ti $3d$-derived band near L, it is nicely shown that the d band is slightly lowered in energy upon cooling down from

 ©2002 The American Physical Society

room temperature. A possible temperature dependence of the Se $4p$ bands at Γ, however, has not been investigated.

Employing high-resolution ARPES with synchrotron radiation we show in this paper that the electronic structure of $1T$-$TiSe_2$ exhibits remarkable changes near the Fermi level in the temperature interval 100 K$\leqslant T \leqslant$300 K. Our analysis of the temperature dependence of the FS topology and band dispersions reveals that both the Ti $3d$ band at L as well as the uppermost Se $4p$ band at Γ are lowered in energy upon cooling. Our photoemission results allow a qualitative understanding of the observed resisitivity anomaly in $1T$-$TiSe_2$ and are discussed with reference to the possible mechanisms underlying the CDW phase transition.

II. EXPERIMENT

The $1T$-$TiSe_2$ crystals were grown by chemical vapor transport using iodine as transport gas and clean surfaces were prepared by cleaving the samples in ultrahigh vacuum. ARPES measurements were carried out at beamlines W3.2 and BW3 at the Hamburger Synchrotronstrahlungslabor (HASYLAB). The incident photons were linearly polarized with the photon polarization and the plane of incidence residing both in the horizontal plane. The angle of incidence was 45°. Photoelectrons were collected with our recently developed spectrometer ASPHERE (angular spectrometer for photoelectrons with high-energy resolution) (Ref. 23) which consists of a 100-mm radius hemispherical deflection analyzer mounted on a two-axis goniometer. Computer-controlled stepper motors enable sequential angle scanned measurements with an absolute angular precision of better than 0.1°. The angular acceptance, which can be adjusted by means of an iris aperture, was set to 1°. The combined (electron and photon) energy resolution was 60 meV for the photoelectron angular distributions (PAD's) and 35 meV for the energy distribution curves (EDC's). The Fermi-level reference was obtained from a polycrystalline gold film that was in electrical contact with the sample. Cooling of the sample was achieved by a two-stage evaporative cooling liquid-helium cryostat and the temperature was measured by two independent sensors, a silicon diode mounted on the cold parts of the cryostat and a platinum resistor glued on the sample holder. The stability and accuracy of the temperature measurement were better than ± 5 K.

III. PHOTOEMISSION RESULTS

A. Fermi-surface mapping

In order to reveal the topology of the electronic structure close to the Fermi level as well as possible changes due to the formation of the CDW we have measured PAD's of $1T$-$TiSe_2$ above (300 K) and below (100 K) the onset temperature of the CDW, i.e., we have recorded the photoemission intensity at constant energy as a function of the surface-parallel momentum $\mathbf{k}_{\|}$. The results for photon energies of 21.2 eV and 78.8 eV are depicted in Fig. 1 where the maps taken at the higher photon energy cover two complete Brillouin zones. In all the maps shown matrix element effects, which are particularly due to the light polarization being

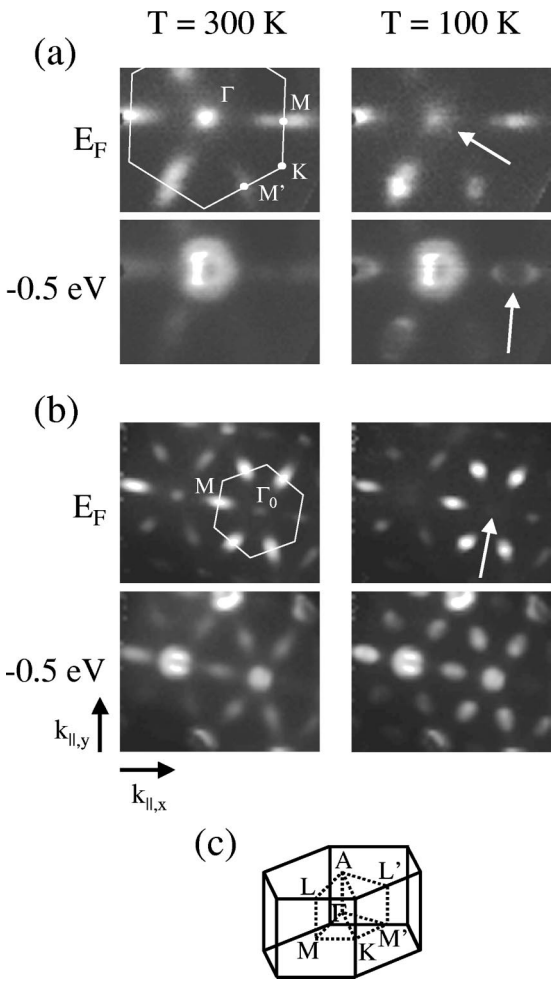

FIG. 1. Constant energy surface mappings of $1T$-$TiSe_2$ taken above (300 K, left panel) and below (100 K, right panel) the onset temperature of the charge-density wave: (a) $h\nu=21.2$ eV and (b) $h\nu=78.8$ eV. The arrows point at the decrease of photoemission intensity in the center of the Brillouin zone and the appearance of a ringlike structure at M, respectively. Photoemission intensity is represented in a linear gray scale with white corresponding to high intensity. (c) Sketch of the Brillouin zone with all relevant high-symmetry points.

fixed with respect to the sample surface, lead to intensity patterns that are characterized by strong intensity variations between equivalent parts of the BZ and thus do not exhibit the trigonal symmetry of the $1T$ structure. Nevertheless, one can clearly see that the FS is made up of six elliptical features centered on the $M(L)$ and $M'(L')$ points and a round structure in the center of the BZ. The first originate from electrons of the Ti $3d$-derived band and the latter is Se $4p$-like in accordance with band-structure calculations.[8–10] At -0.5 eV the Γ-centered emission has developed into a more intense and broader shape, while the photoemission intensity at the BZ boundaries has become very weak. Since the topology of the FS appears to be very similar to that of the isostructural $1T$-$TiTe_2$,[24] which is (semi)metallic due to an indirect p-d band overlap of about 0.6 eV, it is tempting to deduce a corresponding band overlap of roughly 0.5 eV for $1T$-$TiSe_2$ from these maps. This conclusion, however, would

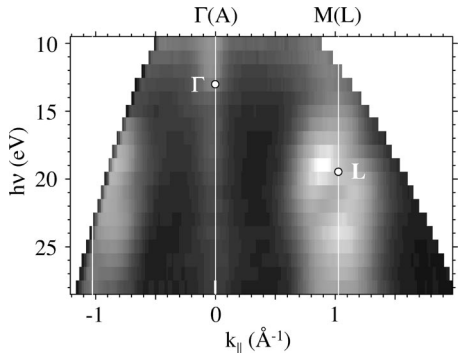

FIG. 2. Photon energy dependent Fermi-surface mapping of $1T$-$TiSe_2$ obtained at room temperature by polar angle scans within the ΓMAL plane of the Brillouin zone. Photoemission intensity is represented in a linear gray scale with white corresponding to high intensity. The Γ and the L point are indicated.

be in striking contrast to previous high-resolution ARPES studies suggesting a very small overlap (<0.12 eV) between the uppermost p band at Γ and the lowest d band at L.[6,7] Hence, the problem of accurately determining the possible band overlap in $1T$-$TiSe_2$ seems to be more complicated and evidently requires measurements in the EDC mode.

The constant energy surfaces mapped at room temperature [Figs. 1(a) and 1(b), left panel] are consistent with those presented in Ref. 7. However, PAD's of $1T$-$TiSe_2$ in the CDW state have not been reported so far. We find that the low-temperature PAD's [Figs. 1(a) and 1(b), right panel] closely resemble the normal-state data except for two remarkable differences. First, the photoemission intensity at the Fermi energy arising from the Se $4p$-like states in the BZ center has become very weak, which could indicate an energy lowering of the related bands. Second, at -0.5 eV the intensity at the $M(L)$ and $M'(L')$ points is slightly enhanced, and for $h\nu=21.2$ eV one can even identify a ringlike structure at some of these points. This may be interpreted as the Se $4p$ bands that are backfolded from the Γ point due to the formation of the $(2\times2\times2)$ superlattice,[5] but again without an analysis of band dispersions by means of EDC's these interpretations remain rather questionable.

The great potential of photoemission intensity mapping is to reveal the topology of the electronic structure close to the Fermi level, i.e., the size and shape of the relevant FS sheets. While the PAD's in Fig. 1 clearly display the relatively small $k_\parallel$ extensions of the Se $4p$- and Ti $3d$-like pockets at the $\Gamma(A)$, $M(L)$, and $M'(L')$ points of the BZ, the photon energy dependent intensity map shown in Fig. 2 demonstrates the $k_\perp$ dispersion of these FS features. To produce this image, we have measured the photoemission intensity at E_F as a function of the photon energy $h\nu$ and momentum $k_\parallel$, i.e., we have performed polar angle scans along the ΓM direction of the BZ for an appropriate range of polar emission angles and photon energies that span the bulk BZ cross section. As the surface-perpendicular momentum $k_\perp$ is implicitly given by the condition that $h\nu$ connects initial and final states in a direct transition, the $h\nu$ axis in Fig. 2 is somehow nonlinearly related to the true $k_\perp$ axis. However, our representation of the measured data is sufficient to state that the FS features exhibit considerable dispersion perpendicular to the layers, which underlines the importance of three-dimensional effects in $1T$-$TiSe_2$ as noted earlier.[6] In spite of some intensity modulations due to matrix elements, a large Ti $3d$-derived ellipsoid centered at L as well as enhanced photoemission intensity around Γ arising from the Se $4p$-like states are well revealed. The assignments of the high-symmetry points of the BZ to photon energies of 13 eV (Γ point) and 19.5 eV (L point) reflect the theoretical band dispersions that always exhibit a Se $4p$ band maximum at Γ and a Ti $3d$ band minimum at L.[8–10] They are corroborated by ARPES measurements in the EDC mode[25] and are in good agreement with previous photoemission studies using synchrotron radiation.[5,6]

From the FS maps of Figs. 1 and 2 we can estimate the volumes of the FS sheets to be about 1% of the full BZ for the Se $4p$ pocket and approximately 6% of the full BZ for all the Ti $3d$ pockets. Hence, we already find evidence for two important conclusions regarding the CDW mechanism of $1T$-$TiSe_2$. First, in view of the small areas of FS available for nesting and the different sizes and shapes of the p- and d-band pockets a simple direct coupling between these pockets within the nesting model seems very unlikely. And second, the larger volume of the d pockets as compared to the p-pocket indicates an imbalance in the number of electrons and holes on the FS, which will reduce possible excitonic insulator effects.

B. Band dispersions near Γ and L

As pointed out in the preceding section, the determination of band overlap, band masses, and band interaction requires photoemission measurements in the EDC mode rather than FS maps. Therefore, we present in Fig. 3 complete ARPES spectra in the ΓMAL plane taken near the Γ and the L point at room temperature (RT) and at 100 K in the CDW phase. The photoemission intensity is visualized by linear gray scale maps in the energy versus $k_\parallel$ plane. The positions of the Se $4p$ emissions and the midpoint of the leading edge are denoted by circles and thin solid lines, respectively.

In the RT data sets [Figs. 3(a) and 3(b)] one can identify the Se $4p$ bands at Γ and the Ti $3d$ band at L, the first exhibiting strong holelike dispersion, the latter showing weaker electronlike dispersion as indicated by the $k_\parallel$ dependence of the leading edge. Fitting second-order polynomials to the experimental dispersions yields band masses of $m_h=-(0.36\pm0.1)m_0$ (m_0 is the mass of a free electron) for the uppermost Se $4p$ band and $m_e=(7\pm2)m_0$ for the Ti $3d$ band. Both values agree very well with previous results.[5,7]

The most striking feature of Fig. 3 is the appearance of an additional band close to the L point in the low-temperature phase [Fig. 3(d)]. Since this band exhibits nearly the same effective mass as the Se $4p$ bands around Γ we may identify it as a p-band that is backfolded due to the formation of the $(2\times2\times2)$ CDW superlattice. This interpretation, which is in line with published data,[5,7] is straightforward, if one bears in mind that the ''old'' L point becomes a Γ point in the reconstructed BZ. Generally, the folding induced by the CDW

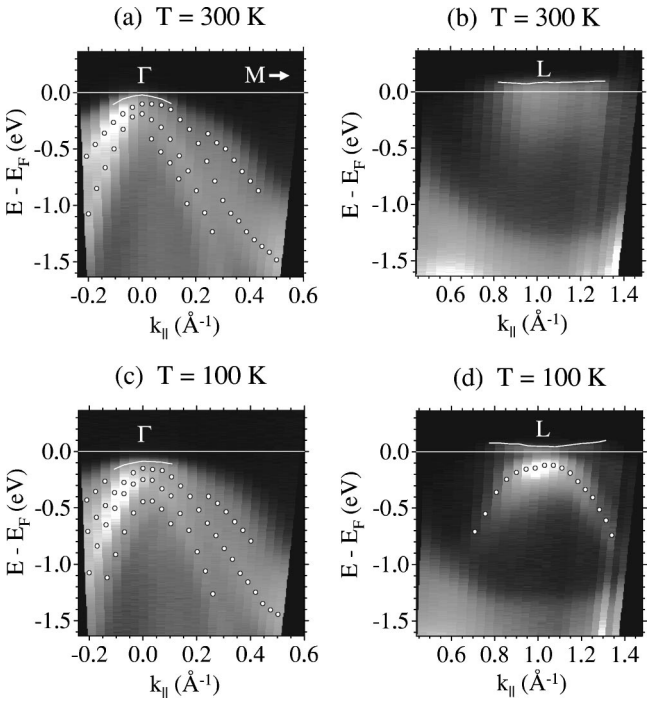

FIG. 3. Energy distribution curves for the Γ*MAL* plane of the Brillouin zone taken with 13 eV [(a) and (c)] and 19.5 eV [(b) and (d)] photons at room temperature [(a) and (b)] and 100 K [(c) and (d)]. Se 4*p* emission features are indicated by circles. Solid lines denote the position of the midpoint of the leading edge. Photoemission intensity is represented in a linear gray scale with white corresponding to high intensity.

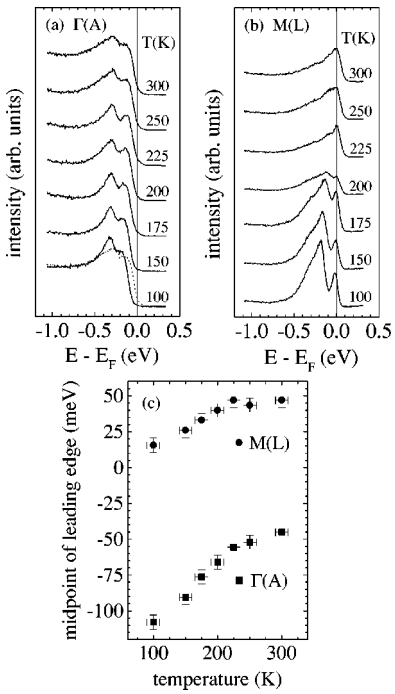

FIG. 4. Temperature-dependent energy distribution curves taken with 21.2 eV photons (a) at normal emission and (b) at the Brillouin-zone boundary. (c) Position of the midpoint of the leading edge as a function of temperature.

superlattice should have only weak effects on the ARPES spectra because the perturbation of the crystal potential is relatively small. In our case, however, the strong effect can probably be explained by *p*-*d* hybridization of the states near Γ leading to a much stronger coupling of the *p* bands to the Ti 3*d* final states at *L*.[5]

Additional evidence for significant *p*-*d* interaction is suggested by the apparent energy lowering of the Se 4*p* bands near Γ in the CDW phase [see Fig. 3(c)]. While in the RT map [Fig. 3(a)] the uppermost *p*-band emissions are grazing the Fermi level, thus indicating the presence of holes on the FS in agreement with previous results,[6] the top of the valence band is clearly shifted by approximately 60 meV towards higher binding energies as the temperature has been decreased to 100 K [Fig. 3(c)]. This effect, experimentally verified here for the first time, can result from a slight repulsion of the *p* and *d* bands at Γ and demonstrates that not only the Ti 3*d* band is affected by the formation of the CDW as noted recently.[7]

In contrast to the Se *p* bands at Γ, the temperature dependence of the Ti 3*d* band at *L* is more difficult to analyze because the *d* emission is strongly affected by the Fermi-Dirac cutoff and the backfolded *p* bands. In a recent high-resolution ARPES study,[7] however, using symmetrized ARPES spectra it was nicely shown that the Ti 3*d* band is situated slightly above the Fermi level at RT, hence only thermally occupied, but shifts into the occupied region upon cooling to 120 K. The energy lowering of the Ti 3*d* band was estimated to be approximately 30 meV that agrees very well with the value of 25 meV we obtain from the shift of the midpoint of the leading edges in Figs. 3(b) and 3(d).

In summary, the temperature induced changes of FS topology in $1T$-$TiSe_2$ appear to be the following: starting at RT with a small number of *p* holes and *d* electrons on the FS, both the uppermost Se 4*p* band at Γ as well as the Ti 3*d* band at *L* are lowered upon cooling, eventually leading to a complete removal of *p* holes from the FS in the CDW phase.

C. Temperature dependence of the valence-band emissions

In order to investigate the evolution of the *p*-*d* band separation in more detail we have taken ARPES spectra of the Se 4*p*-like and Ti 3*d*-like emissions at $\Gamma(A)$ and $M(L)$ in the temperature regime 100 K$\leqslant$T$\leqslant$300 K with $h\nu = 21.2$ eV [Figs. 4(a) and 4(b)]. At this photon energy the corresponding $k_\perp$ is very close to the *L* point, but quite far off the Γ point. However, we assume that the relative changes upon varying the temperature will not too strongly deviate from those at the actual high-symmetry points.

The series of normal emission spectra shown in Fig. 4(a) reveals a double-peak structure related to the spin-orbit split Se 4*p* band at $\Gamma(A)$. Note that contrary to Fig. 3(a) the photoemission intensity exactly at the Fermi energy has decreased to almost zero in the RT data, which demonstrates the effect of $k_\perp$ dispersion upon changing the photon energy from 13 eV to 21.2 eV. As the temperature is decreased, the two peaks shift towards higher binding energies without exhibiting any discontinuity at $T_C \approx 200$ K. Below T_C no indication is found for a backfolded *d* band.

On the other hand, the zone boundary EDC series depicted in Fig. 4(b) shows a superposition of one *d*-band and two *p*-band emissions for low temperatures. From the large asymmetry of the photoemission spectra above T_C one may conclude that the substructure of three peaks already exists at higher temperatures, thus pointing to the fact that the transition is affected by fluctuations over a wide range in temperature.[4] Upon cooling down from RT, the peaks continuously change in intensity and binding energy starting with a predominating Ti 3*d*-like emission above T_C and finally exhibiting very strong Se 4*p*-derived emissions at low temperatures. Apparently, very close to T_C the *p*- and *d*-bands seem to have almost equal spectral weight.

For a more quantitative analysis we display the positions of the midpoint of the leading edge as a function of temperature in Fig. 4(c). If a band lies very close to E_F—as the *p*- and *d*-bands of 1*T*-$TiSe_2$ obviously do—then an energy lowering of this band will naturally result in a corresponding shift of the midpoint of the leading edge. This is illustrated in Fig. 4(c) where the continuous changes with temperature reveal the developing second-order phase transition in the electronic properties of 1*T*-$TiSe_2$. Both the uppermost Se 4*p* band at $\Gamma(A)$ and the Ti 3*d* band at $M(L)$ exhibit the same qualitative behavior: in the temperature interval $T_C \leqslant T \leqslant 300$ K the bands are only slightly lowered in energy, whereas below T_C the bands shift more rapidly towards higher binding energies. The total energy shifts are about 30 meV for the Ti 3*d* band and 60 meV for the Se 4*p* band. However, one should keep clearly in mind that the position of the midpoint of the leading edge is not a measure of the position of the actual band center.

An accurate determination of band positions would require an analysis of the ARPES spectra in terms of line shape fitting, i.e., calculation of an appropriate spectral function, multiplication by the Fermi-Dirac distribution and convolution with the spectrometer response function. We do not intend to present such an analysis here, mainly because of the lack of appropriate self-energy models for CDW systems. Instead, we will rely on arguments that have been put forward in previous ARPES studies:[6,7] (i) From Fig. 4(a) we determine a spin-orbit splitting between the Se 4*p* components of 130 meV at RT and 110 meV at 100 K. Under the assumption of a constant splitting along $\Gamma(A)$ it follows,[6] by addition of these values to the lower component in the spectra taken at Γ ($h\nu = 13$ eV), that the center of the uppermost Se 4*p* band shifts from about 30 meV below E_F at RT to about 130 meV below E_F at 100 K. (ii) In a recent publication[7] the maximum binding energy of the Ti 3*d* band was estimated to be $-(5-10)$ meV at RT and $+(20-25)$ meV at 120 K. These values correspond well to the positions of the Ti 3*d* peak maxima in Fig. 4(b) at RT and 100 K, respectively.

Thus, we arrive at the conclusion that the Se 4*p*–Ti 3*d* band gap between Γ and *L* in 1*T*-$TiSe_2$ increases from about 35 meV to 110 meV upon cooling from RT to 100 K. We have to emphasize that these values are estimated and that the error bars are of the order of 30 meV. Therefore, it is not possible to decide unambiguously whether 1*T*-$TiSe_2$ is semimetallic or semiconducting at RT. But our results definitely show that there is a *p*-*d* band gap with a lower limit of 80 meV at low temperatures (<100 K).

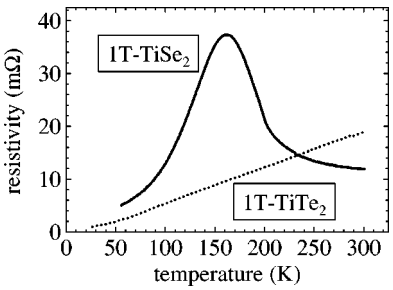

FIG. 5. Electrical resistivity of 1*T*-$TiSe_2$ and 1*T*-$TiTe_2$ as a function of temperature.

IV. DISCUSSION

With regard to the CDW mechanism in 1*T*-$TiSe_2$ we will now try to achieve a qualitative understanding of the characteristic transport properties (electrical resistivity and Hall coefficient) on the basis of our photoemission results. Figure 5 displays the in-plane resistivity ρ measured[26] on a 1*T*-$TiSe_2$ sample that was taken from the same sample charge as the one used in the photoemission experiments. For comparison, we also show a resistivity curve of isostructural 1*T*-$TiTe_2$ which is metallic and exhibits no structural phase transition. Clearly, the resistivity of 1*T*-$TiSe_2$ shows a broad hump superimposed on the metallic background behavior. The resistivity ratio $\rho(165\ \mathrm{K})/\rho(300\ \mathrm{K}) \approx 3.2$ agrees with other published data and indicates rather good sample stoichiometry.[1] The Hall coefficient of 1*T*-$TiSe_2$ has been shown to be positive at RT.[1] Upon cooling it changes sign near 200 K, rapidly decreases until about 100 K, and remains almost constant below.[1]

In a simple two-band model the conductivity and Hall coefficient are given by[1]

$$\sigma = 1/\rho = e(n_h \mu_h + n_e \mu_e), \tag{1}$$

$$R_H = \frac{1}{e} \frac{n_h \mu_h^2 - n_e \mu_e^2}{(n_h \mu_h + n_e \mu_e)^2}, \tag{2}$$

where n_h, n_e, μ_h, μ_e are the densities and mobilities of *p* holes and *d* electrons, respectively. Our room-temperature ARPES data have revealed a small number of Se 4*p* holes at Γ as well as some electrons in the thermally populated Ti 3*d* band at *L*. In fact, we have found the *d*-electron pockets in the FS maps covering a larger volume than the *p*-hole pocket, indicating that $n_e > n_h$. Although this nonstoichiometric electron-hole imbalance is probably due to excess Ti atoms in the van der Waals gaps[13] or due to iodine atoms incorporated in the crystal growth,[27] the defects and excess electrons evidently do not hamper the formation of the CDW. From the band dispersions we have determined an effective mass ratio $m_e/m_h \approx 20$ which, if we assume that no pronounced differences occur in the carrier collision times, will result in a hole mobility μ_h that is about one order of magnitude larger than the electron mobility μ_e. Hence, accord-

ing to Eq. (2) we do get a positive Hall coefficient at RT even though the electron concentration n_e exceeds the hole concentration n_h. Upon cooling both the Se $4p$ band at Γ and the Ti $3d$ band at L are slightly lowered in energy leading to a decrease of n_h and, on account of charge neutrality, of n_e as well. Thus, the resistivity will rise as is indeed observed in Fig. 5. Near $T_C \approx 200$ K the p and d band start to shift more rapidly to higher binding energies, the Hall coefficient changes sign and decreases considerably indicating that the d electrons, in spite of their lower mobility, are becoming the dominant carriers. At the resistivity maximum at about 165 K the Ti $3d$ band has entered the occupied region and the p-d gap has become greater than k_BT so that p holes no longer play a role. Upon further cooling the resistivity starts to decrease because the relaxation rate of the d electrons is reduced due to the lower temperatures. Finally, below about 100 K the resistivity curve appears to reflect normal metallic behavior.

In conclusion, we can successfully explain the transport anomalies in $1T$-$TiSe_2$ by the temperature induced lowering of the Se $4p$ and Ti $3d$ bands near E_F as revealed by photoemission spectroscopy. In particular, we argue that the increase of resistivity with decreasing temperature below RT is caused by the removal of p holes from the FS due to the lowering of the p band and not by the formation of excitons as proposed recently.[7] Although we cannot rule out that excitons are present in the temperature interval 100 K$\leqslant T \leqslant$300 K, their influence will certainly not become dominant. Excitons will only be formed as long as the p-d gap is smaller than the exciton binding energy that is of the order of $k_BT_C \approx 17$ meV. But we have clearly shown that the gap between the Se $4p$ and the Ti $3d$ band continuously increases to about 80 meV upon cooling so that the probability of forming excitons steadily decreases. Therefore, the excitonic insulator mechanism[12–15] can most likely be ruled out as an adequate explanation of the CDW phase transition in $1T$-$TiSe_2$.

In the light of our photoemission results we strongly favor the band-type Jahn-Teller effect for a number of reasons: (i) The top of the Se $4p$ band and the bottom of the Ti $3d$ band are clearly lowered in energy with decreasing temperature. Importantly, these energy shifts become stronger in the CDW phase below T_C [see Fig. 4(c)], which indicates that the gain in electronic energy is indeed caused by the lattice distortion coupled to the CDW and not by the ''normal'' temperature dependence of the electronic energy positions due to lattice contraction. Additionally, the magnitude of the energy shifts appears to be much larger than expected for ''normal'' temperature effects. Within the framework of the Jahn-Teller mechanism two different approaches associated with the two kinds of Ti environments (two different $TiSe_6$ octahedra) in the distortion pattern have been proposed: According to Hughes[16] the rotational motion of the first octahedron towards a trigonal prism is energy lowering in the d bands, whereas Whangbo and Canadell[17] suggested that the structural modulation originates from the p-band energy lowering associated with the Ti–Se bond shortening in the second octahedron. Since the experimentally observed energy lowering is much stronger for the top of the p band than for the bottom of the d band, we strongly favor the picture presented by Whangbo and Canadell. Note that their argumentation does not rely on the presence of electrons in the lowest Ti $3d$ band as Hughes' explanation obviously does. Hence, we may conclude that the CDW phase transition in $1T$-$TiSe_2$ is indeed intrinsic to this compound and is not due to the imperfections whose presence is indicated through the nonstoichiometric occupation of the lowest d band. (ii) The observed band distortions in the electronic structure close to E_F are in rather good agreement with a band-structure calculation for the CDW phase based on the band-type Jahn-Teller effect.[21] In particular, the measured lowering of the Se $4p$-type band at Γ, resulting in a p-d gap of about 100 meV, is reproduced quite well by band theory. (iii) Due to the small FS volumes and the different shapes of the Se $4p$ hole pocket and the Ti $3d$ electron surface direct nesting of these features cannot account for the CDW phase transition. As Motizuki and co-workers[18–21] have shown, a microscopic model based on the band-type Jahn-Teller effect must definitely include strong (wave-vector-dependent) electron-lattice interaction. In fact, the remarkable changes in the electronic structure near E_F due to superlattice formation suggest that electrons and phonons are strongly coupled in $1T$-$TiSe_2$.

We emphasize that due to its peculiar band topology $1T$-$TiSe_2$ is an exception to the transition metal dichalcogenides exhibiting CDW's. Therefore, the CDW phase transitions in other layered compounds may of course be explained by conventional FS nesting[28] or the saddle point mechanism.[29]

V. CONCLUSIONS

Using temperature and photon energy dependent ARPES on the layered charge-density-wave system $1T$-$TiSe_2$, we have accurately measured the three-dimensional FS topology as well as the band dispersions near E_F both in the normal and in the CDW phase ($T_C \approx 200$ K). At room temperature we find a small Se $4p$-type hole surface at Γ and a larger Ti $3d$-type electron surface centered at L. Upon cooling, both the Se $4p$ and the Ti $3d$ band continuously shift towards higher binding energies with the band separation steadily increasing. In the CDW phase at 100 K all Se $4p$ holes are actually removed from the FS and we observe a folding of the Se $4p$ band from Γ to L due to the formation of the $(2\times2\times2)$ superlattice. Our photoemission results provide a direct connection to transport measurements in that they can qualitatively explain the change of sign of the Hall coefficient and the observed resistivity anomaly around 165 K. With regard to the driving force of the CDW phase transition, the results are consistent with the band-type Jahn-Teller mechanism, whereas the scenario of excitonic phases seems very unlikely.

ACKNOWLEDGMENT

We thank C. Teske, O. Seifarth, and J. Riechen for experimental support. This work was supported by the BMBF, Germany (Projects Nos. 05 SB8 FKB and 05 SE8 FKA).

[1] F.J. Di Salvo, D.E. Moncton, and J.V. Waszczak, Phys. Rev. B **14**, 4321 (1976).
[2] K.C. Woo, F.C. Brown, W.L. McMillan, R.J. Miller, M.J. Schaffman, and M.P. Sears, Phys. Rev. B **14**, 3242 (1976).
[3] M.M. Traum, G. Margaritondo, N.V. Smith, J.E. Rowe, and F.J. Di Salvo, Phys. Rev. B **17**, 1836 (1978).
[4] O. Anderson, G. Karschnick, R. Manzke, and M. Skibowski, Solid State Commun. **53**, 339 (1985).
[5] N.G. Stoffel, S.D. Kevan, and N.V. Smith, Phys. Rev. B **31**, 8049 (1985).
[6] O. Anderson, R. Manzke, and M. Skibowski, Phys. Rev. Lett. **20**, 2188 (1985).
[7] Th. Pillo, J. Hayoz, H. Berger, F. Lévy, L. Schlapbach, and P. Aebi, Phys. Rev. B **61**, 16 213 (2000).
[8] A. Zunger and A.J. Freeman, Phys. Rev. B **17**, 1839 (1978).
[9] G.A. Benesch, A.M. Woolley, and C. Umrigar, J. Phys. C **18**, 1595 (1985).
[10] C.M. Fang, R.A. de Groot, and C. Haas, Phys. Rev. B **56**, 4455 (1997).
[11] R.M. White and G. Lucovsky, Nuovo Cimento Soc. Ital. Fis., B **B38**, 280 (1977).
[12] J.A. Wilson, Solid State Commun. **22**, 551 (1977).
[13] J.A. Wilson, Phys. Status Solidi B **86**, 11 (1978).
[14] W. Kohn, Phys. Rev. Lett. **19**, 439 (1967).
[15] B.I. Halperin and T.M. Rice, Rev. Mod. Phys. **40**, 755 (1968).
[16] H.P. Hughes, J. Phys. C **10**, L319 (1977).
[17] M.-H. Whangbo and E. Canadell, J. Am. Chem. Soc. **114**, 9587 (1992).
[18] Y. Yoshida and K. Motizuki, J. Phys. Soc. Jpn. **49**, 898 (1980).
[19] K. Motizuki, Y. Yoshida, and Y. Takaoka, Physica B & C **105**, 357 (1981).
[20] K. Motizuki, N. Suzuki, Y. Yoshida, and Y. Takaoka, Solid State Commun. **40**, 995 (1981).
[21] N. Suzuki, A. Yamamoto, and K. Motizuki, J. Phys. Soc. Jpn. **54**, 4668 (1985).
[22] M. Holt, P. Zschack, Hawoong Hong, M.Y. Chou, and T.-C. Chiang, Phys. Rev. Lett. **86**, 3799 (2001).
[23] K. Rossnagel, L. Kipp, M. Skibowski, and S. Harm, Nucl. Instrum. Methods Phys. Res. A **467**, 1485 (2001).
[24] K. Rossnagel, L. Kipp, M. Skibowski, C. Solterbeck, T. Strasser, W. Schattke, D. Voß, P. Krüger, A. Mazur, and J. Pollmann, Phys. Rev. B **63**, 125104 (2001).
[25] K. Rossnagel, Ph.D. thesis, University of Kiel, 2001.
[26] C. Teske (private communication).
[27] F.J. DiSalvo and J.V. Waszczak, Phys. Rev. B **17**, 3801 (1978).
[28] Th. Straub, Th. Finteis, R. Claessen, P. Steiner, S. Hüfner, P. Blaha, C.S. Oglesby, and E. Bucher, Phys. Rev. Lett. **82**, 4504 (1999).
[29] R. Liu, W.C. Tonjes, V.A. Greanya, C.G. Olson, and R.F. Frindt, Phys. Rev. B **61**, 5212 (2000).